Large eddy simulations of the HyShot II scramjet

J. Larsson, Ronan Vicquelin, I. Bermejo-Moreno

Large eddy simulations of the HyShot II scramjet

By J. Larsson, R. Vicquelin AND I. Bermejo-Moreno

1. Motivation and objective

The present work is part of a broad effort toward predictive simulations of complex flows at high Reynolds numbers. The main objective of the Stanford PSAAP Center (Predictive Science Academic Alliance Program) is to predict the reacting flow in the HyShot II scramjet experiment carried out in the HEG facility of the German Aerospace Agency DLR (cf. Laurence *et al.* 2011). Specifically, the objective is to predict the best-estimate of the flow, to estimate the uncertainties from a range of sources in this prediction, and, finally, to quantify the margin to engine unstart. Unstart occurs in supersonic internal flows when the flow becomes choked (e.g., due to excessive friction or heat addition), which initiates an unsteady unstart process that eventually leads to subsonic flow throughout. The unstart process involves a propagation of shock waves upstream in the combustor, the speed of which depends strongly on the amount of heat addition. The experiments by Laurence *et al.* (2011) indicate propagation velocities of 31 m/s at equivalence ratio (ER) of 0.5, 93 m/s at ER=0.7, and above 200 m/s at ER=1.1. For this problem with fixed mass flux of incoming air, the equivalence ratio is proportional to the fuel mass flux. The length of the HyShot combustor is about 300 mm; thus the unstart process takes about 10 ms at ER=0.5. The experiments were carried out in a shock tube with a test time of about 2.5 ms; thus the unstart process is significantly longer than the test time near the unstart boundary. For this reason, it is clear that shock tube experiments can not give a precise unstart bound. An alternative approach is to use a validated large eddy simulation (LES) method to explore and determine the unstart bound. This is the approach taken here, and the motivation of the work described in this brief.

The complexity of the flow (turbulence, shocks, mixing, combustion) implies that a careful multi-stage validation plan is needed. Moreover, the available quantitative experimental data for the HyShot case is limited to measurements of pressure (mean and rms) and heat transfer (although these are highly uncertain) along two lines in the combustor. Therefore, validation on the HyShot problem alone is not sufficient. The first step in the validation is to compute a supersonic flat plate boundary layer as a basic check on the LES method and, specifically, the modeling of the friction and heat transfer at the wall. The wall-modeling approach itself was validated in Kawai & Larsson (2012); in the present brief we specifically validate the implementation in the unstructured code *Charles* (cf. Khalighi *et al.* 2011). The next validation step is the duct flow with shock/boundary layer interactions studied experimentally by Helmer & Eaton (2011). This problem validates the capability of the wall-modeled LES to capture stress-induced secondary corner flows and, most importantly, shock/boundary layer interaction; preliminary results from this validation exercise are described in Bermejo-Moreno *et al.* (2011) elsewhere in this volume. The third validation problem is the experiments of the so-called 'CESCo' model combustor by Gamba *et al.* (2011). These experiments are ongoing, and will include both toluene PLIF thermometry measurements of the cold flow (described by Miller *et al.* 2011 elsewhere in this volume) and several quantitative measurements of the reacting flow problem. The application of the LES methodology to this problem is part of

ongoing work. The final step is to apply the LES method to the HyShot II combustor; preliminary results of this are shown in this brief.

2. Methodology

The filtered compressible Navier-Stokes equations are solved for the conserved variables. For reacting flow, the total energy E is defined as the sum of sensible, kinetic and chemical energy. The residual subgrid stress is modeled using an eddy-viscosity hypothesis together with the model by Vreman (2004). The subgrid heat flux and species transport are modeled using gradient hypotheses with fixed turbulent Prandtl and Schmidt numbers, both taken as 0.5. The equations are implemented in the unstructured code *Charles*, which uses a solution-adaptive approach inspired by Larsson & Lele (2009) in which a non-dissipative scheme with low aliasing error is used away from shock waves while an unstructed essentially non-oscillatory (ENO) second-order accurate shock-capturing scheme is applied near discontinuities. At each time step, the shock-capturing scheme is applied if the negative rate of dilatation $-\partial_j u_j > \max\left(1.5\sqrt{\omega_j\omega_j}, 0.05\,c/h\right)$, where ω_j is the vorticity and c/h is the speed-of-sound divided by the cell size. For reacting flows, the shock-capturing scheme is additionally applied if two adjacent cells differ by more than 300 K in temperature, by more than 0.4 in the mixture fraction, or by more than 0.3 in the mass fraction of H_2O.

2.1. *Combustion model*

The Stanford H_2/O_2 mechanism (9 species, 20 reactions) by Hong *et al.* (2011) is used to model the chemical reactions together with a steady flamelet/progress-variable method (Pierce & Moin 2004). The FlameMaster code† is used to compute a sequence of steady diffusion flamelets in a counterflow setting. The flamelets are computed at a pressure of 1.5 bar with temperatures set to 300 K and 1300 K on the fuel and air sides, respectively. These values are representative of the conditions in the HyShot combustor, but hydrodynamic effects will naturally produce different pressures and temperatures at different locations of the flame front. In the present work we follow the approach of Terrapon *et al.* (2010), where the species mass fractions are assumed to be independent of the pressure and temperature (at the flamelet boundaries), whereas the source term of the reaction progress variable is assumed to scale with the square of pressure (since the majority of the reactions are bimolecular). This is a rather crude assumption and is the subject of ongoing work.

The effect of turbulence on the small-scale chemistry is modeled by a presumed β probability distribution function for the mixture fraction Z. For the reaction progress variable C, a delta distribution is assumed. At the macro-scale (LES) level, additional transport equations are solved for the filtered mixture fraction $\widetilde{Z}$, the subfilter variance $\widetilde{Z''Z''}$ and the filtered progress variable $\widetilde{C}$.

2.2. *Wall-model*

The boundary layers in HyShot II are about 0.5 mm thick in the isolator, growing to 1-1.5 mm farther downstream. The friction Reynolds number of the boundary layers varies from 1500 to 4000; with reasonable resolution of the viscous length scale this implies that a grid of order $100{\cdot}10^9$ points would be needed with traditional (wall-resolved) LES. Since this is completely impractical, one might wonder whether it is possible to obtain

† Developed by Heinz Pitsch.

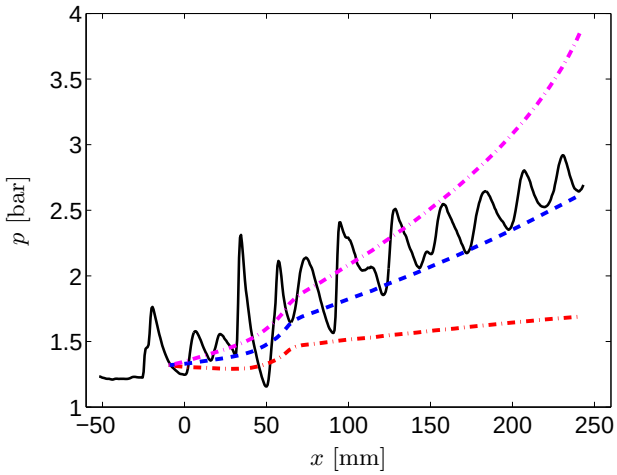

FIGURE 1. Rayleigh-Fanno analysis of pressure increase in the HyShot II combustor. Pressure on the lower wall from RANS (solid) compared with the Rayleigh-Fanno result with integrated heat release, friction and wall heat losses (dashed). Also shown are the Rayleigh-Fanno results without the friction component (dash-dotted, lowest pressure-rise) and without the wall heat losses (dash-dotted, highest pressure-rise).

reasonable predictions of the flow by simply ignoring the viscous near-wall region, i.e., to knowingly under-resolve this region. After all, if the pressure rise is due to the heat release, which occurs in the mixing layer between the fuel jet and the surrounding air, then perhaps the near-wall processes are not important?

To answer this question we utilize a simple Rayleigh-Fanno analysis, i.e., inviscid 1D flow of a perfect gas with heat addition and friction. Figure 1 shows the pressure on the lower wall from RANS and the equivalent Rayleigh-Fanno result with heat release, heat losses and friction taken from the RANS. The latter obviously does not include non-uniform 3D effects or shock waves, but nevertheless gives a similar pressure rise. Within the Rayleigh-Fanno framework it is then straightforward to compute the pressure rises without the effects of wall friction or wall heat losses; these are also shown in the figure. The effect of these phenomena on the pressure rise is dramatic. The 'true' pressure rise is 1.3 bar; neglecting friction causes a -0.9 bar difference whereas neglecting wall heat losses causes a +1.3 bar difference. The conclusion is that near-wall processes are of paramount importance in this scramjet flow, and thus they must be accurately predicted by the LES. This is accomplished by using a wall-model.

The wall-model used here is taken from the work of Kawai & Larsson (2012), who both extended the previously existing equilibrium-stress approach to compressible flows with wall heat transfer and proposed a novel idea for how to minimize the error in the predicted skin friction. The wall-model is defined by the two ODEs

$$\frac{d}{dn}\left[(\mu+\mu_t)\,\frac{dU_\parallel}{dn}\right] = 0\,, \tag{2.1a}$$

$$\frac{d}{dn}\left[(\mu+\mu_t)\,U_\parallel\frac{dU_\parallel}{dn} + c_p\left(\frac{\mu}{Pr}+\frac{\mu_t}{Pr_t}\right)\frac{dT}{dn}\right] = 0\,, \tag{2.1b}$$

where n is a local wall-normal coordinate; $U_\parallel$ is the velocity magnitude locally parallel to the wall; and μ, c_p, Pr, and T are the viscosity, specific heat at constant pressure, Prandtl number and temperature, respectively. The eddy viscosity μ_t used in the wall-model is

taken from a mixing-length hypothesis as

$$\mu_t = \kappa\rho n\sqrt{\frac{\tau_w}{\rho}}\left[1-\exp\left(\frac{-n^+}{A^+}\right)\right]^2, \tag{2.2}$$

where ρ and τ_w are the density and wall shear stress, respectively. We note that $\sqrt{\tau_w/\rho}$ is the velocity scale in a boundary layer with varying mean density, and that $n^+ \equiv \sqrt{\rho_w\tau_w}n/\mu_w$. The modeling parameters are taken as $\kappa = 0.41$, $Pr_t = 0.9$, and $A^+ = 17$, which leads to a log-law intercept of 5.2. Following the results of Kawai & Larsson (2012), the wall-model is solved in the lowest 10% of the boundary layer (based on δ_{99}).

3. Results

In this section we first present results of the validation study of a flat plate boundary layer, followed by preliminary results on the full reacting HyShot II scramjet combustor. An additional validation study on the flow in a duct with shock/boundary layer interaction is described in Bermejo-Moreno *et al.* (2011) elsewhere in this volume.

3.1. *Validation on supersonic flat plate boundary layer*

The supersonic flat plate boundary layer experiment by Souverein *et al.* (2010) is considered here. The free-stream Mach number is 1.69 and the Reynolds number is $Re_\theta \approx 50,000$ (based on momentum thickness), $Re_\delta \approx 620,000$ (based on boundary layer thickness), and $Re_\tau \approx 10,000$ (based on friction velocity). We emphasize that this is a much higher Reynolds number than what traditional wall-resolved LES is capable of computing.

The computational domain is $53 \times 10 \times 4$ in terms of the boundary layer thickness at the inlet δ_0 in the streamwise, wall-normal, and spanwise directions, respectively. The boundary layer thickness δ at the station where statistics are compared is $\delta \approx 1.3\delta_0$. The grid resolution in the boundary layer is $(\Delta x, \Delta y_w, \Delta z)/\delta = (0.10, 0.025 \rightarrow 0.04, 0.05)$. In viscous units, the grid resolution is $(\Delta x^+, \Delta y^+, \Delta z^+) \approx (1100, 270 \rightarrow 450, 550)$.

The inflow turbulence is synthetically generated using the technique of Touber & Sandham (2009), which allows for the Reynolds stresses and a length scale to be specified. The results are compared with experimental data near the end of the domain, where the flow is fully developed and has reached the correct Reynolds number.

The mean velocity is shown in Fig. 2 and agrees well with the log-law without any significant "log-layer mismatch" as is common in wall-modeled LES (Kawai & Larsson 2012). The LES results also agree well with the incompressible data of Degraaff & Eaton (2000). The data of Souverein *et al.* (2010) is offset by about two units. The agreement between the two measurement techniques employed in that study suggests that the offset is not a measurement error. One plausible explanation is that wall (in the experiment) was not fully adiabatic, since the van Driest transformation is known to be flawed for cooled walls.

The resolved Reynolds stresses are shown in Fig. 3 and compared with several sets of experimental data. The agreement with the incompressible data of Klebanoff (1955) is nearly perfect, except for in the first few grid points adjacent to the wall. The errors in the first few grid points near the wall are inescapable in wall-modeled LES (Kawai & Larsson 2012); more importantly, the results show that these errors do not contaminate the solution away from the wall.

The LES results agree reasonably well with the incompressible data of Degraaff &

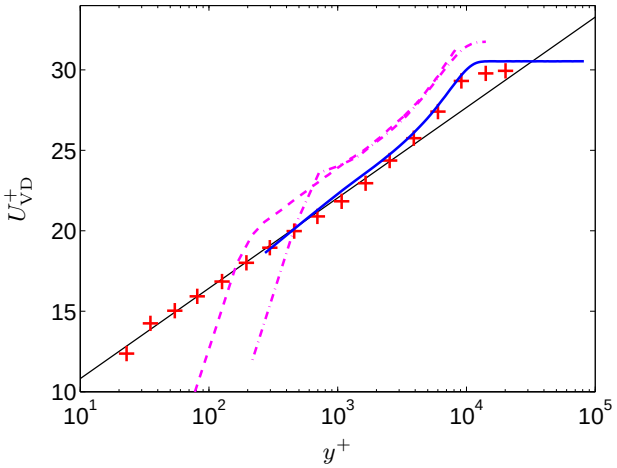

FIGURE 2. van Driest transformed mean velocity profile (solid) compared with the log-law $\ln(y^+)/0.41 + 5.2$ (thin), experiments by Souverein *et al.* (2010) using dual-PIV (dash-dotted) and zoom-PIV (dashed), and incompressible experiments by Degraaff & Eaton (2000) at $Re_\theta = 31,000$ (plusses).

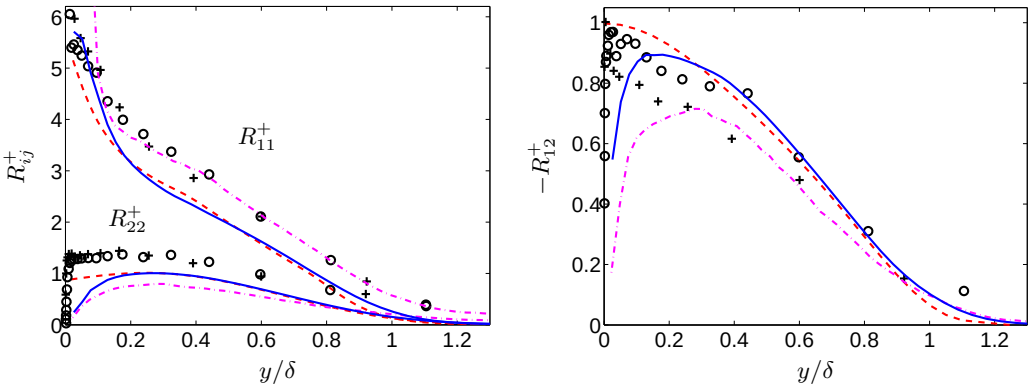

FIGURE 3. Resolved Reynolds stresses $R^+_{ij} = \widetilde{\overline{\rho} u''_i u''_j}/\tau_w$ from wall-modeled LES (solid) compared with experiments at the same conditions by Souverein *et al.* (2010) (dash-dotted) and to incompressible experiments by Klebanoff (1955) at $Re_\theta = 50,000$ (dashed) and Degraaff & Eaton (2000) at $Re_\theta = 31,000$ (plusses) and $Re_\theta = 13,000$ (circles). Left: Normal stresses R_{11} and R_{22}. Right: Shear stress R_{12}.

Eaton (2000), with good agreement for the shear stress but underpredictions for the normal stresses. The latter is, at least, consistent with the notion of the LES only resolving parts of the turbulence spectrum. Finally, the supersonic data of Souverein *et al.* (2010) is lower than the LES (and the other experiments) in the shear stress and wall-normal stress; this is especially true in the first 20-30% near the wall. Because the measured shear-stress profile is inconsistent with a high-Reynolds number boundary layer, we must conclude that there is some measurement error in that data set.

Overall, this flat plate validation test shows that the wall-modeled LES methodology is capable of accurately predicting a boundary layer at a Reynolds number that is representative of realistic engineering devices, while using a grid where the cell size is completely determined by outer length scales (i.e., not the viscous one).

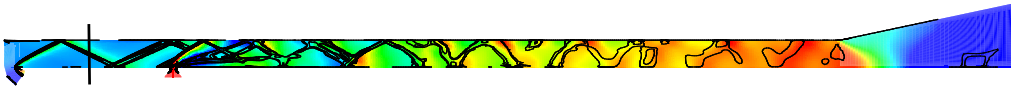

FIGURE 4. Slice through the injector from a RANS simulation. Contours of pressure showing the increase caused by combustion, overlayed with contour lines of large negative dilation showing the strongest shocks. The vertical line before the injector shows the location of the inflow for the LES simulations.

3.2. *Preliminary results for HyShot II scramjet*

Figure 4 shows a RANS result for the reacting flow in the HyShot II scramjet. The shock-trap and leading edge of the lower wall are visible at the far left of the figure, as is the fuel injector about 50 mm farther downstream. The domain for the LES is chosen to start between these two locations, at the vertical line in Fig. 4. There are several reasons for choosing this point as the LES inlet. To minimize the cost, the inlet should be as close to the injector as possible, but sufficiently far upstream that the inflow turbulence becomes developed and the injector bow shock is captured properly. In addition, the inlet should not be placed at a point where the oblique shock-train is near the wall, where a shock/boundary layer interaction occurs. Having chosen the inlet location, the inflow profiles are taken from RANS and used in the synthetic turbulent inflow generation.

The full HyShot II combustor is 75 mm wide with four fuel injectors spaced equidistantly. Only a single injector (i.e., 1/4 of the full combustor width) is computed with LES, assuming periodic boundary conditions in the spanwise direction. This approximation is expected to be reasonable, since Terrapon *et al.* (2010) showed relatively minor effects of the combustor side walls in their RANS study. The walls are assumed isothermal at 300 K due to the short duration of the shock-tube experiments. The total pressure and temperature of the hydrogen are 5 bar and 300 K, respectively, and correspond to nominal conditions for the experiment.

The grid is fully structured with a total of $14 \cdot 10^6$ cells. The spanwise grid spacing is $\Delta z = 0.15$ mm throughout the domain. The streamwise grid spacing Δx is 0.30 mm at the inlet and in the combustor, but smoothly refined down to 0.15 mm around the injector. The wall-normal grid spacing Δy is 0.04 mm at the walls and 0.12 mm in the core. Naturally, the grid is finer in the injector itself, which has a diameter of 2 mm. The boundary layers are approximately 1 mm thick throughout most of the domain (although thinner near the inlet); thus the grid resolution is very coarse in the boundary layers, with only 4-7 cells per δ_{99} in the streamwise and spanwise directions. This is not expected to give grid-independent results following the criteria in Kawai & Larsson (2012), and further grid refinements will be necessary in the future. Note that the wall-model is not applied in the injector itself, since the flow there is laminar due to the strong contraction.

The simulations are run for about 100,000 time steps, corresponding to a total time of 9 ms; slightly longer than the actual test time in the shock tube. The simulations are run on 192 processors for a total of 90 hours, or 17,000 core-hours. The relatively low cost is entirely due to the wall-model, which not only enables the use of a very coarse grid, but also allows for the use of large time steps by eliminating the need for very thin cells (that resolve the viscous sublayer) adjacent to walls.

An instantaneous snapshot is shown in Fig. 5. The multiple incoming oblique shock

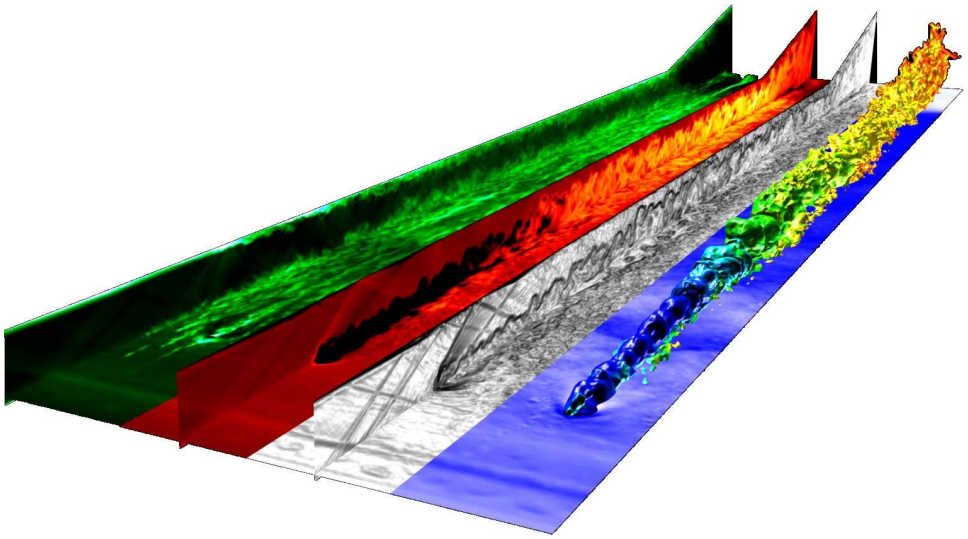

FIGURE 5. Instantaneous snapshot from LES of the HyShot II combustor. The computational domain (one injector) is replicated four times in the spanwise direction. From the left, the slices show contours of streamwise velocity u_1, temperature T, simulated Schlieren $|\nabla\rho|$, and pressure p. In addition, the right-most section shows an isosurface at the stoichiometric mixture fraction, colored by the OH concentration.

waves are visible in the Schlieren image, as is the strong bow shock around the fuel injector. The fuel jet is initially relatively unperturbed, but breaks down in full turbulence farther downstream. The velocity contours show the thin incoming boundary layers and how these grow farther downstream. Finally, the temperature contour shows how the heat release leads to increased temperatures downstream, up to about 2500 K before the nozzle.

The quantitative experimental data available are measurements of pressure and heat flux along lines on the lower and upper walls in the combustor. A total of 9 shots under reacting conditions were measured; for each shot the mean and rms of the quantities are available. The comparison between this data and the LES results is shown in Figs. 6–8. Since the LES is computed at nominal conditions, which approximately correspond to the average among the 9 experimental shots, the comparison is made with respect to this average. The minimum and maximum among the 9 shots are also shown, which combine the effects of measurement uncertainty and shot-to-shot variation.

The mean pressure is shown in Fig. 6, and agrees rather closely with the experimental data. However, the results also show how the shocks are overly smeared in the downstream half of the combustor. The most likely reason for this is the grid resolution, which as mentioned before is rather coarse.

The rms pressure fluctuations are shown in Fig. 7 and agree quite well with the measured data. The fact that p_{rms} is not overly damped, despite the smeared shock waves, is due to the use of a solution-adaptive switch: the shock-capturing scheme is only used around shocks, and the turbulence is relatively unaffected by the shock-capturing dissipation.

The final quantity available from the experiment is the wall heat flux, which is shown in Fig. 8. The agreement is reasonable but not perfect. The reason for this is not clear,

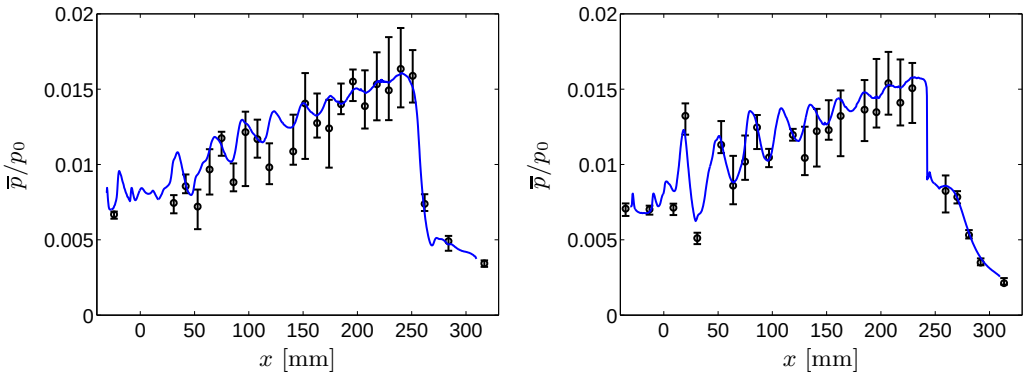

FIGURE 6. Mean wall pressure along lines halfway between injectors in HyShot II from LES (solid) compared with shock tube experiment from DLR (Laurence *et al.* 2011). Average experimental value (circles) and the min/max (errorbars) among the 9 shots. Scaled by the total pressure p_0 in the shock tube for each shot. Left: Lower wall. Right: Upper wall.

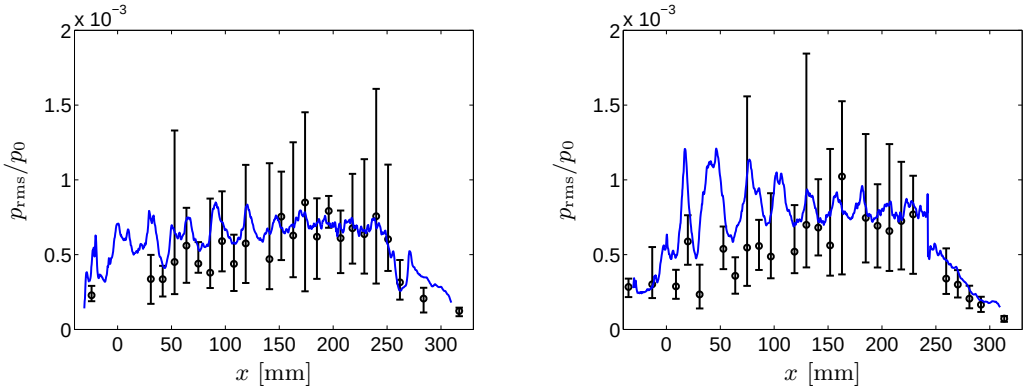

FIGURE 7. Rms wall pressure fluctuation along lines halfway between injectors in HyShot II from LES (solid) compared with shock tube experiment from DLR (Laurence *et al.* 2011). Average experimental value (circles) and the min/max (errorbars) among the 9 shots. Scaled by the total pressure p_0 in the shock tube for each shot. Left: Lower wall. Right: Upper wall.

although it is known from prior work (Kawai & Larsson 2012) that the present grid resolution in the boundary layers is marginal at best.

Having compared the LES results with the available experimental data, we next visualize some aspects of the flow. Figure 9 shows the full computational domain including the nozzle. The mean reaction progress variable clearly shows how the flame is lifted, with vigorous burning starting about 50 mm downstream of the injector on average. While difficult to see in the figure, there is a small recirculation region upstream of the fuel injector where burning occurs; this provides some burned gases to the shear layer, which is necessary for flame stabilization in the flamelet/progress-variable modeling approach. The lifted flame is consistent with the instantaneous source term of H_2O (the mass fraction of which is the progress variable), which is primarily large in the region 30–70 mm downstream of the injector. Behind this region, burning occurs in the shear layers of the fuel jet. The burning essentially ceases in the nozzle due to the rapid decrease of pressure,

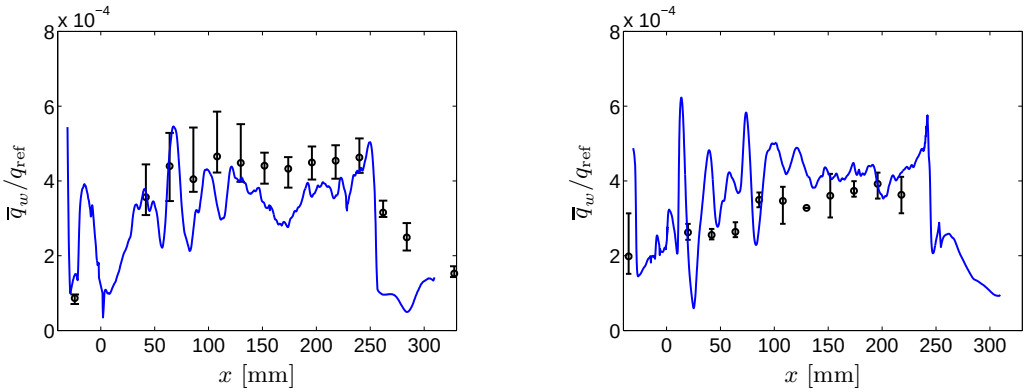

FIGURE 8. Mean wall heat flux along lines through the injector in HyShot II from LES (solid) compared with shock tube experiment from DLR (Laurence *et al.* 2011). Average experimental value (circles) and the min/max (errorbars) among the 9 shots. Scaled by a reference heat flux $q_{\rm ref} = \sqrt{p_0}(h_0 - h_w)$ for each shot, where h_0 is the total enthalpy in the shock tube (for each shot), and h_w is the enthalpy at the cold walls. Left: Lower wall. Right: Upper wall.

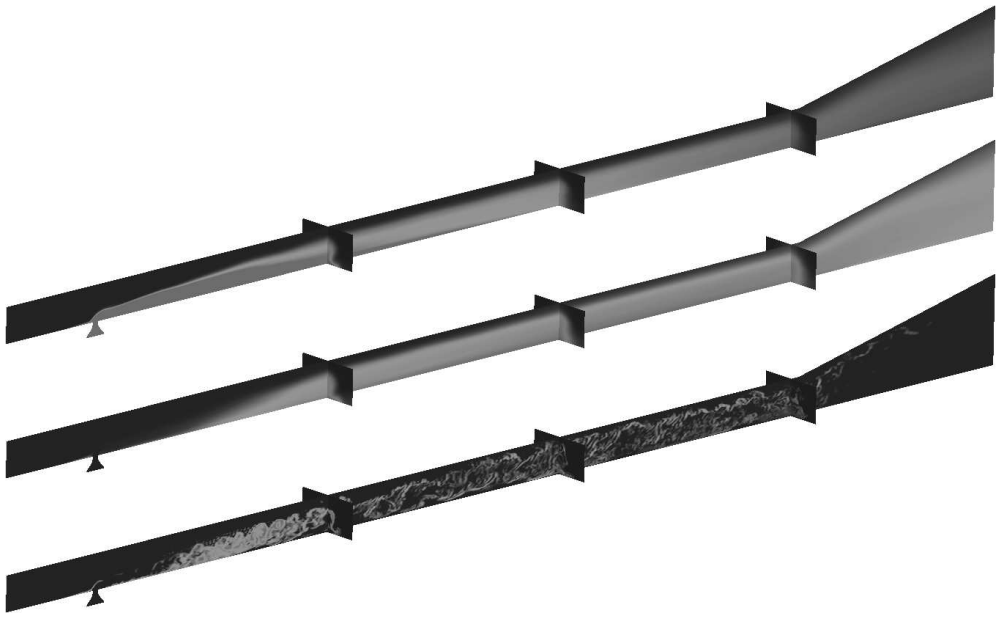

FIGURE 9. Combustion results from LES of the HyShot II combustor. Contours on a slice through the injector and three slices normal to the flow at x =80, 160 and 240 mm. Top: Mean mixture fraction from 0 to 0.1 (dark to light), where the stoichiometric mixture fraction is 0.028. Middle: Mean progress variable (H_2O mass fraction) from 0 to 0.24 (dark to light). Bottom: Instantaneous source of progress variable on a logarithmic scale (dark to light).

which has a direct effect on the reaction rates. By the end of the domain, 80% of the H_2 has been converted into H_2O.

The experimental campaign at DLR included some limited OH^* chemiluminescence imaging (e.g., Fig. 6 in Laurence *et al.* 2011). To compare with this experimental image, a mechanism for OH^* formation (taken from the JetSurF 2.0 mechanism, Wang *et al.*

FIGURE 10. Composite simulated Schlieren $|\nabla\rho|$ in a slice through the injector and line-of-sight integrated mean OH^* chemiluminesce in the first half of the combustion chamber.

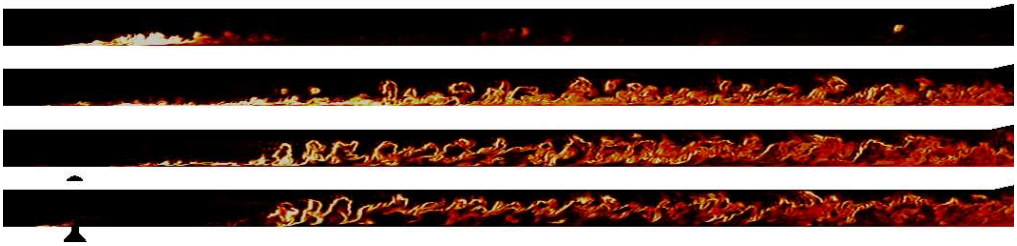

FIGURE 11. Instantaneous OH^* chemiluminesce in vertical slices at different spanwise locations. From bottom to top: $z = 0$ (through the injector), $z = 2$ mm, $z = 4$ mm, and $z = 9.375$ mm (halfway between the injectors).

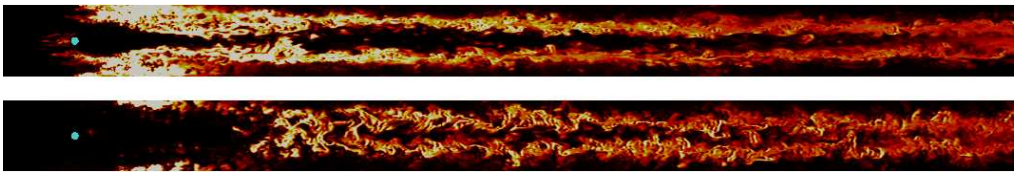

FIGURE 12. Instantaneous OH^* chemiluminesce in horizontal planes at different heights above the lower wall of $y = 0.5$ mm (upper figure) and $y = 2$ mm (lower figure).

2010) is included in the flamelet model. A composite Schlieren and average line-of-sight integrated OH^* is shown in Fig. 10. Note that line-of-sight integration (in the spanwise direction) is done to emulate the experimental measurement. Comparison with Fig. 6 in Laurence *et al.* (2011) shows several similarities between the LES and the experiment, most importantly the vigorous burning near the wall and the increased height of the reacting region after the second shock impingement. The major discrepancy is that the LES shows a very vigorous burning region immediately behind the injector, whereas the experiment is essentially non-burning there.

This is seen more clearly in Figs. 11–12, which show the instantaneous OH^* emissions. The high OH^* signal immediately behind the injector in Fig. 10 is due to strong burning between the injectors, where the bow shocks meet. Whether this strong burning at heights of about half the boundary layer thickness is physical is unclear. Specifically, the fact that the wall is strongly cooled combined with the lack of temperature effects on the chemistry in the present flamelet model suggests caution. This is issue is part of ongoing and future work.

4. Summary and future work

This brief describes ongoing work toward predictive large eddy simulations of the reacting and high Reynolds number flow in the HyShot II scramjet combustor. Although the preliminary results are promising, specifically the pressure statistics and the moderate computational cost, much work remains to be done.

The first step is to investigate whether improvements can be made to the shock-capturing scheme, thus yielding sharper shocks. Any improvements must preserve the robustness of the method. Although the solution-adaptive nature of the method confines the shock-capturing errors to narrow regions around shock waves, it is nevertheless clear that a better shock-capturing scheme would generate sharper shocks. Following the theoretical analysis of Larsson (2010), this should also have a positive effect on the accuracy of the post-shock turbulence and mixing.

The next step will be to refine the grid until grid convergence is achieved for the key statistics. The affordable cost of the present simulations implies that much finer grids can be used.

Finally, we will explore the unstart bound by computing cases at different fuel injection rates. Very long simulations may be needed to determine whether unstart occurs, given how slow the unstart process is near the bound. Such long simulations should be possible, since the present simulations actually cover a longer time than the test time in the shock tube.

Acknowledgments

This work is supported by the Department of Energy Predictive Science Academic Alliance Program (PSAAP; grant DE-FC52-08NA28614). The work on wall-modeling is supported by the Air Force Office of Scientific Research (grant FA9550-11-1-0111). Computational time has been provided by the Dept. of Energy under the ERCAP and INCITE programs, as well as on the local Certainty cluster funded by the NSF MRI-R2 program.

REFERENCES

Bermejo-Moreno, I., Larsson, J., Campo, L., Bodart, J., Vicquelin, R., Helmer, D. & Eaton, J. 2011 Wall-modeled large-eddy simulation of shock/turbulent boundary-layer interaction in a duct. In *Annu. Res. Briefs*. Center for Turbulence Research.

Degraaff, D. B. & Eaton, J. K. 2000 Reynolds-number scaling of the flat-plate turbulent boundary layer. *J. Fluid Mech.* **422**, 319–346.

Gamba, M., Miller, V. A., Mungal, M. G. & Hanson, R. K. 2011 Ignition and flame structure in a compact inlet/scramjet combustor model. AIAA Paper 2011-2366.

Helmer, D. & Eaton, J. 2011 Measurements of a three-dimensional shock-boundary layer interaction. *Tech. Rep.* TF-126. Flow Physics and Computational Engineering, Department of Mechanical Engineering, Stanford University.

Hong, Z., Davidson, D. F. & Hanson, R. K. 2011 An improved H2/O2 mechanism based on recent shock tube/laser absorption measurements. *Combust. Flame* **158**, 633–644.

Kawai, S. & Larsson, J. 2012 Wall-modeling in large eddy simulation: length scales, grid resolution and accuracy. *Phys. Fluids*, to appear.

Khalighi, Y., Nichols, J. W., Lele, S., Ham, F. & Moin, P. 2011 Unstructured large eddy simulation for prediction of noise issued from turbulent jets in various configurations. AIAA Paper 2011-2886.

Klebanoff, P. 1955 Characteristics of turbulence in a boundary layer with zero pressure gradient. Tech. report. NASA.

Larsson, J. 2010 Effect of shock-capturing errors on turbulence statistics. *AIAA J.* **48** (7), 1554–1557.

Larsson, J. & Lele, S. K. 2009 Direct numerical simulation of canonical shock/turbulence interaction. *Phys. Fluids* **21**, 126101.

Laurence, S. J., Schramm, J. M., Karl, S. & Hannemann, K. 2011 An experimental investigation of steady and unsteady combustion phenomena in the HyShot II combustor. AIAA Paper 2011-2310.

Miller, V. A., Gamba, M., Mungal, M. G. & Hanson, R. K. 2011 Toluene planar laser-induced fluorescence thermometry and flow visualization of compressible flows in an expansion tube. In *Annu. Res. Briefs*. Center for Turbulence Research.

Pierce, C. D. & Moin, P. 2004 Progress-variable approach for large-eddy simulation of non-premixed turbulent combustion. *J. Fluid Mech.* **504**, 73–97.

Souverein, L. J., Dupont, P., Debieve, J. F., Dussauge, J. P., van Oudheusden, B. W. & Scarano, F. 2010 Effect of interaction strength on unsteadiness in turbulent shock-wave-induced separations. *AIAA J.* **48** (7), 1440–1493.

Terrapon, V. E., Pecnik, R., Ham, F. & Pitsch, H. 2010 Full-system RANS of the HyShot II scramjet. Part 2: Reactive cases. In *Annu. Res. Briefs*, pp. 69–80. Center for Turbulence Research.

Touber, E. & Sandham, N. 2009 Large-eddy simulation of low-frequency unsteadiness in a turbulent shock-induced separation bubble. *Theor. Comp. Fluid Dyn.* **23**, 79–107.

Vreman, A. W. 2004 An eddy-viscosity subgrid-scale model for turbulent shear flow: Algebraic theory and applications. *Phys. Fluids* **16** (10), 3670–3681.

Wang, H., Dames, E., Sirjean, B., Sheen, D. A., Tangko, R., Violi, A., Lai, J. Y. W., Egolfopoulos, F. N., Davidson, D. F., Hanson, R. K., Bowman, C. T., Law, C. K., Tsang, W., Cernansky, N. P., Miller, D. L. & Lindstedt, R. P. 2010 A high-temperature chemical kinetic model of n-alkane (up to n-dodecane), cyclohexane, and methyl-, ethyl-, n-propyl and n-butyl-cyclohexane oxidation at high temperatures, JetSurF version 2.0 (http://melchior.usc.edu/jetsurf/jetsurf2.0).